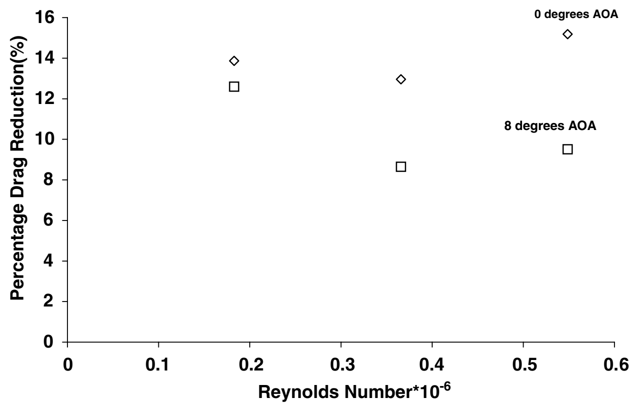

Fig. 7 Percentage drag reduction on the ellipsoid with coating.

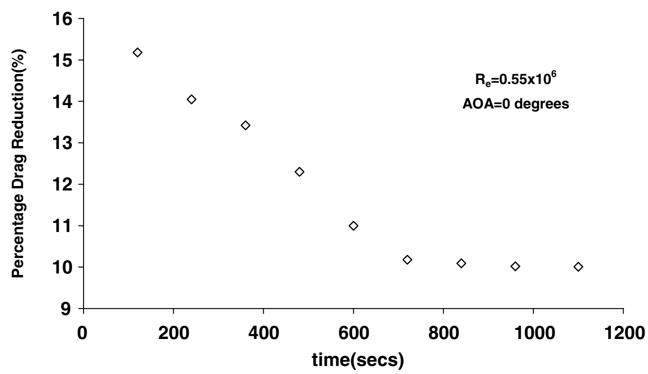

Fig. 8 Percentage drag reduction as a function of time.

period of time and is allowed to dry. The results presented here are for models that have remained submerged for 1100 s.

Conclusions

A hydrophobic coating/skin was tested to quantify its effectiveness as a hydrodynamic drag reduction device. PIV performed on a flat plate, with and without the coating, showed a 20% drag reduction induced by the coating. Drag measurement tests, conducted on a 3-ft-long ellipsoid model in the water tunnel, showed 14 and 10% drag reductions at 0- and 8-deg model angle of attack, respectively. Drag reduction levels drop with time, apparently approaching a limiting value after 15 min.

Acknowledgments

The authors thank C. Neinhuis of the University of Bonn and his students for helping with initial samples of the skin and providing information about suppliers of the raw materials for the fabrication of the skin.

References

[1]Bushnell, D. M., "Turbulent Drag Reduction for External Flows," AIAA Paper 83-0227 and AIAA Paper 83-0231, Jan. 1983.

[2]Bandopadhyay, P. R., "REVIEW—Mean Flow in Turbulent Boundary Layers Distributed to Alter Skin Friction," *Journal Fluids Engineering*, Vol. 108, 1986, pp. 127–140.

[3]Bandopadhyay, P. R., "Convex Curvature Concept of Viscous Drag Reduction," *Viscous Drag Reduction in Boundary Layers*, edited by D. M. Bushnell and J. N. Hefner, Vol. 123, Progress in Aeronautics and Astronautics, AIAA, Washington, DC, 1990, pp. 285–324.

[4]Gad-el-Hak, M., "Flow Control," *Applied Mechanics Reviews*, Vol. 9, 1989, pp. 447–468.

[5]Bruse, M., Bechert, D. W., Van der Hoeven, J. G. T., Hage, W., and Hoppe, G., "Experiments with Conventional and Novel Adjustable Drag-Reducing Surfaces," *Near-Wall Turbulent Flows*, edited by R .M. C. So, C. G. Speziale, and B. E. Launder, Elsevier, New York, 1993, pp. 719–738.

[6]Jung, W. J., Mangiavacchi, N., and Akhavan, R., "Suppression of Turbulence in Wall-Bounded Flows by High-Frequency Spanwise Oscillations," *Physics of Fluids*, Vol. 4, No. 8, 1992, pp. 1605–1607.

[7]Bandopadhyay, P. R., "Development of a Microfabricated Surface for Turbulence Diagnostics and Control," *Application of Microfabrication to Fluid Mechanics*, FED Vol. 1997, American Society of Mechanical Engineers, Fairfield, NJ, 1994, pp. 63–70.

[8]William, B. B., "Wall Slip and Boundary Effects in Polymer Shear Flows," Ph.D. Dissertation, Dept. of Chemical Engineering, Univ. of Wisconsin, Madison, WI, May 2000.

[9]Barthlott, W., and Neinhuis, C., "Purity of the Sacred Lotus, or Escape from Contamination in Biological Surfaces," *Planta*, Vol. 202, 1997, pp. 1–8.

[10]Neinhuis, C., and Barthlott, W., "Characterization and Distribution of Water-Repellent, Self-Cleaning Plant Surfaces," *Annals of Botany*, Vol. 79, 1997, pp. 667–677.

[11]Adam, N. K., "Principles of Water-Repellency," *Waterproofing and Water-Repellency*, edited by J. L. Moilliet, Elsevier, Amsterdam, 1963, pp. 1–147.

[12]Kline, S. J., and McClintock, F. A., "Describing Uncertainties in Single-Sample Experiments," *Mechanical Engineering*, Vol. 75, Jan. 1953, pp. 3–88.

[13]Willert, C. E., and Gharib, M., "Digital Particle Image Velocimetry," *Experiments in Fluids*, Vol. 10, 1991, pp. 181–193.

[14]Singh, K., "Development of Image Processing Algorithms for an Improved Particle Image Velocimetry System," M.S. Thesis, Dept. of Aerospace Engineering, Texas A&M Univ., College Station, TX, May 1998.

[15]Ahn, S., "An Experimental Study of Flow over a 6 to 1 Prolate Spheroid at Incidence," Ph.D. Dissertation, Aerospace Engineering Dept., Virginia Polytechnic Inst. and State Univ., Blacksburg, VA, Oct. 1992.

P. R. Bandyopadhyay
Associate Editor

Optimized Boundary Treatment of Curved Walls for High-Order Computational Aeroacoustics Schemes

Jonghoon Bin,* Cheolung Cheong,† and Soogab Lee‡
Seoul National University,
Seoul 151-742, Republic of Korea

Introduction

AN accurate simulation of acoustic scattering and radiation from arbitrary bodies is one of the important goals in the field of computational aeroacoustics. These problems require not only a high-resolution numerical scheme but also accurate boundary treatment. In this Note, we develop a high-order wall boundary treatment that can be readily applied with a high-order finite difference in computational aeroacoustics.

There are mainly three types of approaches for treating complex geometries. The first is to use a conventional structured grid, the second is to make use of unstructured grids that create irregular numerical interfaces all over the physical domain, and the last type is to use so-called Cartesian grid methods.[1–11] Most of these schemes have been developed for steady-state, transonic flow or low-order accuracy. However, acoustic waves are intrinsically unsteady, and

Received 20 May 2001; revision received 6 March 2003; accepted for publication 10 September 2003.

*Ph.D. Candidate, School of Mechanical and Aerospace Engineering; mrbin@snu.ac.kr.

†BK21 Postdoctoral Research Associate, School of Mechanical and Aerospace Engineering; accu99@snu.ac.kr.

‡Professor, School of Mechanical and Aerospace Engineering; solee@plaza.snu.ac.kr. Senior Member AIAA.

their amplitudes are several orders smaller than the mean flow with the frequencies generally in the level of kilohertz. As a result, not only high-order numerical scheme but also high-order boundary conditions are required for simulating aeroacoustic phenomena.[12]

The objectives of this study are twofold. The main objective is to present a new optimized high-order boundary treatment using Cartesian coordinates and to examine the effectiveness of interpolation for the ghost point near the boundary from the standpoint of a wave number. The second objective is to present a new optimized interpolation for a variable or its derivatives in the neighborhood of grid points with high-order accuracy. The method proposed in this Note provides the high-order accuracy required in the interpolation of physical values.

Numerical Methodology

Consider the approximation of the unknown value $X(x_j, \eta)$ at $x_j + \eta\Delta x$ of a uniform grid where $-1 < \eta < 1$ and $\Delta x = x_j - x_{j-1}$. Suppose M values of f to the right and N values of f to the left are used to form the unknown value $X(x_j, \eta)$, that is, $f(x_j + \eta\Delta x)$ or $\partial f(x_j + \eta\Delta x)/\partial x$ if the accuracy of finite difference scheme is retained up to the 4th order:

$$X(x_j, \eta) = \sum_{k=-N}^{M} a_k f_{j+k} \qquad (M + N + 1 = 7) \tag{1}$$

To determine the coefficients a_k of Eq. (1), expand the right-hand side of Eq. (1) in a Taylor series of Δx by equating coefficients of the same powers of Δx up to fourth-order accuracy:

$$\begin{bmatrix} m_{11} & m_{12} & m_{13} & m_{14} & m_{15} & m_{16} & m_{17} \\ m_{21} & & m_{23} & & m_{25} & & m_{27} \\ & \ddots & & \ddots & & \ddots & \\ \vdots & \vdots & \vdots & \vdots & \vdots & \vdots & \vdots \\ m_{51} & m_{52} & m_{53} & \cdots & m_{55} & \cdots & m_{57} \end{bmatrix} \begin{bmatrix} a_1 \\ a_2 \\ a_3 \\ a_4 \\ a_5 \\ a_6 \\ a_7 \end{bmatrix} = \begin{bmatrix} b_1 \\ b_2 \\ \vdots \\ \vdots \\ b_5 \end{bmatrix} \tag{2}$$

If two coefficients to be used for the optimizing process are left when the matrix $C_j, j = 1, \ldots, 7$, that is, $C_j = \{m_{1j}\ m_{2j}\ m_{3j}\ m_{4j}\ m_{5j}\}^T$ is jth column of left-hand-side (LHS) matrix A_{ij}, $1 \le i \le 5$, $1 \le j \le 7$, and right-hand-side (RHS) matrix of equation is $\mathrm{RHS}_i(\eta)$, the preceding equations are represented into the following matrix form:

$$C_2 a_2 + C_4 a_4 + C_5 a_5 + C_6 a_6 + C_7 a_7 = -C_1 a_1 - C_3 a_3 + \mathrm{RHS}_i(\eta) \tag{3}$$

When the matrices $K = \{C_2\ C_4\ C_5\ C_6\ C_7\}$ and $Y = \{a_2\ a_4\ a_5\ a_6\ a_7\}^T$ are defined and the inverse matrix of K is multiplied by each side of Eq. (3), the following equation is obtained:

$$Y = -K^{-1} C_1 a_1 - K^{-1} C_3 a_3 + K^{-1} \mathrm{RHS}_i(\eta), \qquad i = 1, \ldots, 5 \tag{4}$$

Then two unknown variables are left. The unknown coefficients are determined by requiring the Fourier transform of the values on the RHS of Eq. (1) to be a close approximation of the values on the LHS.

If $f(x)$ is given as a periodic function, its Fourier transform is $\tilde{f}(\alpha)$, where α is the wave number. Here $f(x)$ is related to $\tilde{f}(\alpha)$ by the inverse Fourier transform formula

$$f(x) = \int_{-\infty}^{\infty} \tilde{f}(\alpha) \exp(i\alpha x)\, \mathrm{d}\alpha \tag{5}$$

In Eq. (5), the absolute value and the argument of $\tilde{f}(\alpha)$ are denoted by $A(\alpha)$ and $\phi(\alpha)$. Therefore, Eq. (5) may be rewritten as

$$f(x) = \int_{-\infty}^{\infty} A(\alpha) \exp\{i[\alpha x + \phi(\alpha)]\}\, \mathrm{d}\alpha \tag{6}$$

A wave number analysis of large stencil finite difference schemes[13,14] has shown that finite difference schemes are accurate only over a limited band of low wave numbers or large wavelengths. We will also consider an interpolation process that remains high-order accurate over a required wave number range, that is, $0 \le \alpha\Delta x \le \kappa$. Here, waves with unit amplitude over the desired band of wave numbers are considered, that is, $A(\alpha) = 1$.

The Fourier transforms of the LHS and RHS of Eq. (1) are

$$\tilde{X}(\alpha\Delta x, \eta) = \left[\sum_{k=-N}^{M} a_k \exp(i\alpha k\Delta x)\right] \tilde{f} \tag{7}$$

where $\tilde{X}$ is Fourier transform of $X(x_j, \eta)$.

The local error $E_{\mathrm{local}}(\alpha\Delta x, \eta)$ is defined as the square amplitude of the difference between the LHS and RHS of Eq. (7) after performing a Fourier transform:

$$E_{\mathrm{local}}(\alpha\Delta x, \eta) = \left|\tilde{X}(\alpha\Delta x, \eta) - \sum_{k=-N}^{M} a_k \exp(i\alpha k\Delta x)\right|^2 \tag{8}$$

The total integrated error over the band of wave number $0 \le \alpha\Delta x \le \kappa$ is

$$E_{\mathrm{total}} = \int_0^{\kappa} \left|\tilde{X}(\alpha\Delta x, \eta) - \sum_{k=-N}^{M} a_k \exp(i\alpha k\Delta x)\right|^2 \mathrm{d}(\alpha\Delta x) \tag{9}$$

It is possible to combine the traditional truncated Taylor series in Eq. (4) with the optimized finite difference approximation in Eq. (9). These free parameters can then be fixed into certain values to minimize the integrated error E_{total}:

$$\frac{\partial E}{\partial a_1} = \frac{\partial E}{\partial a_3} = 0 \tag{10}$$

Here E_{total} is a function of the parameter κ and η, and the parameter κ can be adjusted to the optimized overall results.

Optimized Wall Boundary Treatment

In this section, a new method for boundary treatment, which is stable while it retains higher-order accuracy, is proposed:

$$\boldsymbol{V} \cdot \hat{n}_{\mathrm{wall}} = \frac{\partial p}{\partial \hat{n}_{\mathrm{wall}}} = 0 \tag{11}$$

The wall boundary condition (11) will be enforced by the ghost values of pressure suggested by Tam et al.[14] Most enforcement points, however, are not on mesh points. Therefore, information about the pressure gradient at these boundary points can only be obtained by interpolation. In addition, their interpolation accuracy must be at least higher than that used in high-order finite difference schemes to avoid the errors from their interpolation. In this work, a two-step process is carried out. The first step is the interpolation process for the values of pressure normal to the surface, that is, two–seven points. The next step is the optimizing process to determine ghost points of pressure, that is, one point, for satisfying wall boundary condition in Fig. 1.

If a seven-point stencil finite difference method is used, the process to obtain the values of pressure normal to the surface, that is, the six interior interpolation pressure points 2–7, is as follows. The procedure for determining the value of pressure at index 4 in Fig. 1 is briefly introduced as an example. The values of pressure in line A or B at time level n(a1–a7 or c1–c7) should be determined by high-order interpolation approaches described earlier as shown in Fig. 2. The seven points a1–a7 in Fig. 2 are approximated one dimensionally in the y direction and are calculated through the high-order interpolation method suggested in this Note. Here, the values of pressure at the unknown points, that is, points a1–a7, are calculated by the seven-point approximation in Eq. (1), with either central difference in the interior regions or backward difference in the boundary regions, where the central differences are not applied

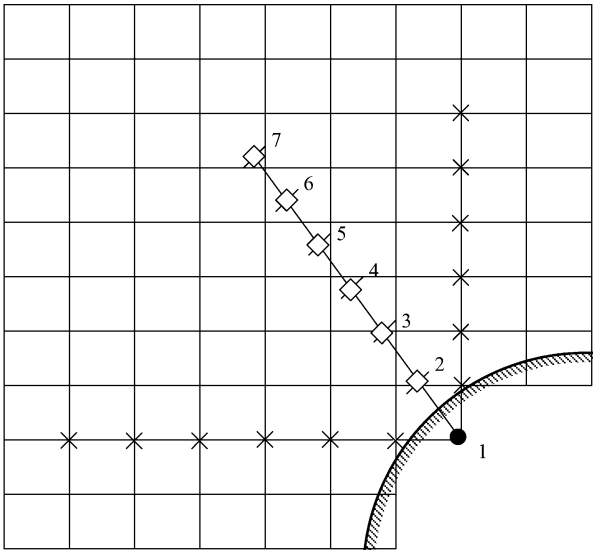

Fig. 1 Wall boundary region from a circular cylinder: ◇, interpolation pressure points and ●, ghost point.

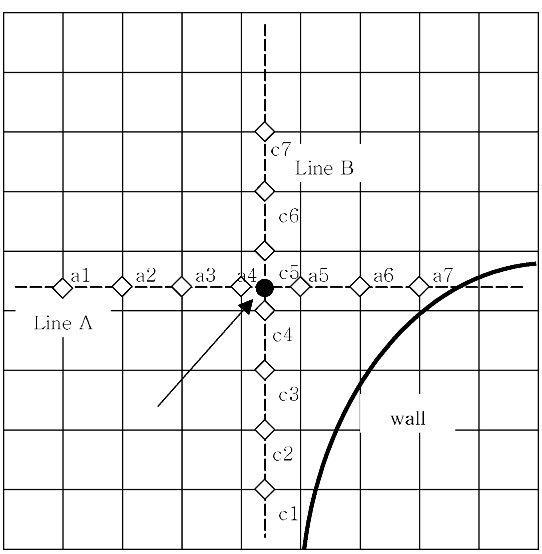

Fig. 2 Interpolation process in a interior region: ●, interpolation point and ◇, extra points.

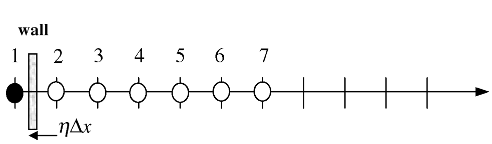

Fig. 3 Classification of wall boundary treatment: ○, interpolated pressure points and ●, ghost point.

due to the existence of the rigid wall. The value of pressure at index 4 is obtained by using these values of pressure in points a1–a7 with the same approximation explained earlier. These interpolated values of interior points in Fig. 1, that is, points 2–7, will be used for the optimized wall boundary treatment. All of the procedures could be developed and implemented automatically with a computer program.

Because the boundary point might not be located on the grid, as shown in Fig. 3, the ghost values for the wall boundary are expressed as follows as described in the preceding section with an accuracy of order $\mathcal{O}(\Delta x^4)$ if the methods described earlier are utilized:

$$\frac{\partial f}{\partial x}(x_i + \eta\Delta x) = \frac{1}{\Delta x}\sum_{j=1}^{7} a_j f_{i-2+j} \tag{12}$$

It is possible to combine the traditional truncated Taylor series with a finite difference approximation so that coefficients a_j can easily be determined. The coefficient can be obtained from the truncated Taylor series up to the order of $(\Delta x)^4$:

$$\begin{bmatrix} 1 & 1 & 1 & 1 & 1 & 1 & 1 \\ \Delta_{-1} & 0 & \Delta_1 & \Delta_2 & \Delta_3 & \Delta_4 & \Delta_5 \\ \frac{\Delta_{-1}^2}{2!} & 0 & \frac{\Delta_1^2}{2!} & \ddots & \frac{\Delta_3^2}{2!} & \ddots & \frac{\Delta_5^2}{2!} \\ \vdots & \vdots & \vdots & \vdots & \vdots & \vdots & \vdots \\ \frac{\Delta_{-1}^4}{4!} & 0 & \frac{\Delta_1^4}{4!} & \cdots & \frac{\Delta_3^4}{4!} & \cdots & \frac{\Delta_5^4}{4!} \end{bmatrix} \begin{bmatrix} a_1 \\ a_2 \\ a_3 \\ a_4 \\ a_5 \\ a_6 \\ a_7 \end{bmatrix} = \begin{bmatrix} 0 \\ 1 \\ \eta\Delta x \\ \frac{(\eta\Delta x)^2}{2!} \\ \frac{(\eta\Delta x)^3}{3!} \end{bmatrix} \tag{13}$$

$$E_{\text{local}}(\eta, \alpha\Delta x) = |\alpha\Delta x \cdot \exp\{i[\alpha(\eta\Delta x)]\} - G(a_j, \alpha\Delta x)|^2 \tag{14}$$

where $G(a_j, \alpha\Delta x) = [a_1\exp(-i\alpha\Delta x) + a_2 + a_3\exp(i\alpha\Delta x) + a_4\exp(2i\alpha\Delta x) + a_5\exp(3i\alpha\Delta x) + a_6\exp(4i\alpha\Delta x) + a_7\exp(5i\alpha\Delta x)]$ and $\kappa = 1.1$.

When Eq. (10) is applied, all of the coefficients in Eq. (12) are determined. Finally Eqs. (11) and (12) provide ghost point of pressure at index 1 in Fig. 1. The entire process is performed at time level n, and then the variables ρ, u, v, and p are updated.

Numerical Applications

A. Reflection of Two-Dimensional Acoustic Waves

A test simulation was performed to validate the accuracy of the schemes and wall boundary conditions for a problem involving sound propagation and reflection. The acoustic disturbance is generated by an initial acoustic pulse and is governed by the linearized Euler equations:

$$p = \hat{p}\exp\left(-\ell\mathrm{n}(2)\left\{\left[(x - x_s)^2 + (y - y_s)^2\right]\big/ b^2\right\}\right) \tag{15}$$

where the amplitude $\hat{p}$, b, and position (x_s, y_s) are 0.1, $3\Delta x$, and (0.0, -3.0), respectively. In the numerical simulation, the mesh sizes are chosen to be $\Delta x = \Delta y = 0.05$ with a time step of $\Delta t = 0.001$. Figure 4 shows the propagation and the reflection of acoustic pulse near the wall in the $\eta = -0.9$ case defined in Eq. (1) and shown in Fig. 3.

B. Sound Scattering Problem

To show the accuracy of this treatment, the case of scattering of a time-periodic acoustic source by a single cylinder is investigated. All of the calculations are executed with the following conditions: $\Delta x = \Delta y = 1.0$, $\Delta t = 0.01$, and $\omega = 0.1\pi$. Figure 5 shows the instantaneous pressure contour of the scattering of the plane wave at $t = 200$ and of the time-periodic acoustic wave at $t = 195$. Figure 5 shows a zero pressure contour of the two cases. We can find easily that there is good agreement between the numerical results and the exact solutions.

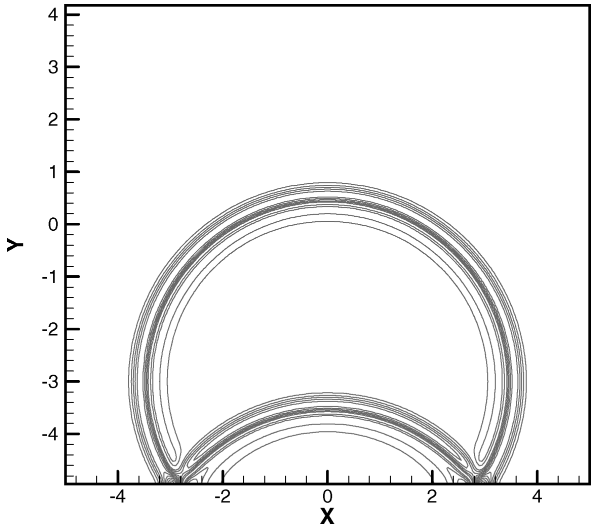

Fig. 4 Reflection of acoustic pulse near the rigid wall $\eta = -0.9$ case; pressure contour at time $t = 3.5$.

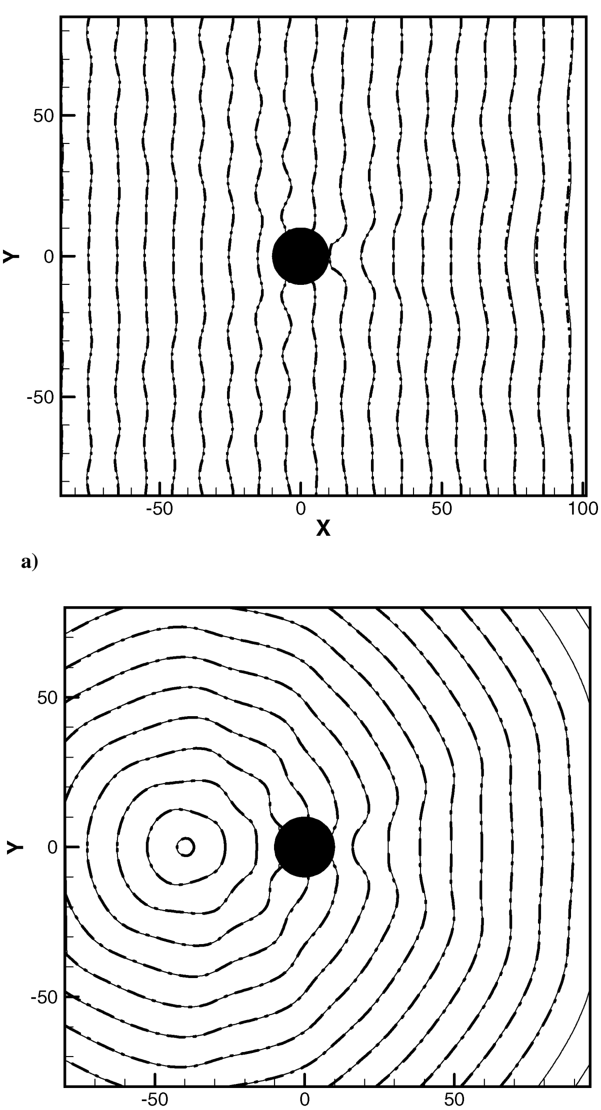

Fig. 5 Zero pressure contour: a) scattering of plane wave, $t = 200$ and b) scattering of time-periodic acoustic wave, $t = 195$: ——, numerical solution and —·—, analytic solution.

Conclusions

A newly developed Cartesian boundary treatment of solid surfaces for acoustic scattering and radiation problems has been presented for use in conjunction with high-order finite difference schemes, in particular the seven-point stencil finite difference scheme.[12] The acoustic modeling of scattering from an infinitely long rigid cylinder is investigated to evaluate the performance, effectiveness, and accuracy of this boundary treatment.

The ghost values for the wall boundary condition are determined so that the slip wall boundary condition is satisfied at the boundary surface. All of the numerical simulations are performed on Cartesian coordinates and are compared with analytic solutions. There is a good agreement between the numerical results and the exact solutions for several standard benchmark problems.[12,13] Furthermore, this approximation is also efficient because the number of operations along the wall boundaries account for only a small part of the overall computational load.

Acknowledgment

This work was supported by the International Cooperation Research Program of the Ministry of Science and Technology.

References

[1]Cheong, C., and Lee, S., "Grid-Optimized Dispersion-Relation-Preserving Schemes on General Geometries for Computational Aeroacoustics," *Journal of Computational Physics*, Vol. 174, 2001, pp. 246–276.

[2]Peskin, C. S., "Flow Patterns Around Heart Valves: A Numerical Method," *Journal of Computational Physics*, Vol. 10, 1972, pp. 252–271.

[3]LeVeque, R. J., and Li, Z., "The Immersed Interface Method for Elliptic Equations with Discontinuous Coefficients and Singular Sources," *SIAM Journal of Numerical Analysis*, Vol. 31, 1994, pp. 1019–1044.

[4]Li, Z., "A Note on Immersed Interface Methods for Three Dimensional Elliptic Equations," *Computers and Mathematics with Applications*, Vol. 31, 1996, pp. 9–17.

[5]Briscolini, M., and Santangelo, P., "Development of the Mask Method for Incompressible Unsteady Flows," *Journal of Computational Physics*, Vol. 84, 1989, pp. 57–75.

[6]Goldstein, D., Handler, R., and Sirovich, L., "Modeling a No-Slip Flow Boundary with an External Force Field," *Journal of Computational Physics*, Vol. 105, 1993, pp. 354–366.

[7]Saiki, E. M., and Biringen, S., "Numerical Simulation of a Cylinder in Uniform Flow: Application of a Virtual Boundary Method," *Journal of Computational Physics*, Vol. 123, 1996, pp. 450–465.

[8]Li, Z., and Lai, M.-C., "The Immersed Interface Method for the Navier–Stokes Equations with Singular Forces," *Journal of Computational Physics*, Vol. 171, 2001, pp. 822–842.

[9]Young, D. P., Melvin, R. G., Bieterman, M. B., Johnson, F. T., Sammant, S. S., and Bussoletti, J. E., "A Locally Refined Rectangular Grid Finite-Element Method : Application to Computational Fluid Dynamics and Computational Physics," *Journal Computational Physics*, Vol. 92, 1991, pp. 1–66.

[10]Powel, K. G., and De Zeeuw, D., "An Adaptively Refined Cartesian Mesh Solver for the Euler Equations," *Journal of Computational Physics*, Vol. 104, 1993, pp. 56–68.

[11]Quirk, J. J., "An Alternative to Unstructured Grids for Computing Gas Dynamic Flows Around Arbitrarily Complex Two-Dimensional Bodies," *Computers and Fluids*, Vol. 23, No. 1, 1994, pp. 125–142.

[12]Tam, C. K. W., "Computational Aeroacoustics: Issues and Methods," *AIAA Journal*, Vol. 33, 1995, pp. 1788–1796.

[13]Kurbatskii, K. A., and Tam, C. K. W., "Cartesian Boundary Treatment of Curved Walls for High-Order Computational Aeroacoustics Schemes," *AIAA Journal*, Vol. 35, 1997, pp. 133–140.

[14]Tam, C. K. W., and Dong, Z., "Wall Boundary Conditions for High Order Finite Difference Schemes in Computational Aeroacoustics," *Journal of Theoretical Computational Fluid Dynamics*, Vol. 6, 1994, pp. 303–322.

H. M. Atassi
Associate Editor